Trapping and desorption of complex organic molecules in water at 20 K

Article (Published Version)

Trapping and desorption of complex organic molecules in water at 20 K

Daren J. Burke, Fabrizio Puletti, Paul M. Woods, Serena Viti, Ben Slater, and Wendy A. Brown

Citation: The Journal of Chemical Physics **143**, 164704 (2015); doi: 10.1063/1.4934264
View online: http://dx.doi.org/10.1063/1.4934264
View Table of Contents: http://scitation.aip.org/content/aip/journal/jcp/143/16?ver=pdfcov
Published by the AIP Publishing

Trapping and desorption of complex organic molecules in water at 20 K

Daren J. Burke,[1,a)] Fabrizio Puletti,[2] Paul M. Woods,[3] Serena Viti,[4] Ben Slater,[2] and Wendy A. Brown[1]

[1]*Division of Chemistry, University of Sussex, Falmer, Brighton BN1 9QJ, United Kingdom*
[2]*Department of Chemistry, University College London, 20 Gordon Street, London WC1H 0AJ, United Kingdom*
[3]*Astrophysics Research Centre, School of Mathematics and Physics, Queen's University Belfast, University Road, Belfast BT7 1NN, United Kingdom*
[4]*Department of Physics and Astronomy, University College London, Gower Street, London WC1E 6BT, United Kingdom*

(Received 17 August 2015; accepted 9 October 2015; published online 26 October 2015)

The formation, chemical, and thermal processing of complex organic molecules (COMs) is currently a topic of much interest in interstellar chemistry. The isomers glycolaldehyde, methyl formate, and acetic acid are particularly important because of their role as pre-biotic species. It is becoming increasingly clear that many COMs are formed within interstellar ices which are dominated by water. Hence, the interaction of these species with water ice is crucially important in dictating their behaviour. Here, we present the first detailed comparative study of the adsorption and thermal processing of glycolaldehyde, methyl formate, and acetic acid adsorbed on and in water ices at astrophysically relevant temperatures (20 K). We show that the functional group of the isomer dictates the strength of interaction with water ice, and hence the resulting desorption and trapping behaviour. Furthermore, the strength of this interaction directly affects the crystallization of water, which in turn affects the desorption behaviour. Our detailed coverage and composition dependent data allow us to categorize the desorption behaviour of the three isomers on the basis of the strength of intermolecular and intramolecular interactions, as well as the natural sublimation temperature of the molecule. This categorization is extended to other C, H, and O containing molecules in order to predict and describe the desorption behaviour of COMs from interstellar ices. © *2015 AIP Publishing LLC.* [http://dx.doi.org/10.1063/1.4934264]

I. INTRODUCTION

Complex organic molecules (COMs), defined as molecules containing 6 or more atoms,[1] are becoming increasingly important in astrophysical studies. With the technological advances of telescope arrays such as ALMA, COMs are being readily detected in a wider range of astrophysical environments such as hot cores and corinos,[2] low mass protostars,[3] and comets.[4] It was originally assumed that COMs were primarily formed as a result of gas phase chemistry. However, in common with small molecules such as water and CO_2, the role of surface processes within molecular ices is becoming increasingly important to account for the abundances of COMs in several astrophysical regions.[5] As a result, there has been an increasing focus on the study of COMs in the laboratory. In particular, there have been investigations of the thermal processing of glycolaldehyde, methyl formate, and acetic acid[6–8] and studies of the molecular formation pathways of glycolaldehyde,[9–11] ethylene glycol,[11] and methyl formate,[12,13] amongst others.[14]

The three isomers of $C_2O_2H_4$ (glycolaldehyde, methyl formate, and acetic acid) are an important group of COMs, given their classification as potential pre-biotic species. Glycolaldehyde is the simplest of the monosaccharide sugars and is a key intermediate in the formose reaction, involving the formation of sugars, polyols, and hydroxy acids from formaldehyde. The formose reaction yields ribose, which is a central constituent of RNA.[15] Acetic acid is also an important pre-biotic species as it is a precursor to the formation of glycine. Methyl formate is the most simple ester detected in astrophysical environments and it has been proposed that its presence is closely linked to the formation of dimethyl ether, another important COM, by reaction of methanol.[16]

Astrochemical modelling has shown that glycolaldehyde, methyl formate, and acetic acid are all readily formed within icy mantles in the interstellar medium (ISM).[5,17–20] These ices contain a wide range of simple and complex molecules,[21] with the most abundant species being water ice, comprising up to 70% of the ice depending on the astrophysical environment. Laboratory studies have shown that the dominant water component has a profound effect on the constituents of model interstellar ices. It has been readily shown that smaller volatiles within these ices, such as CO, CO_2, and CH_4, are retained within water ice beyond their natural sublimation temperatures and are released at the amorphous to crystalline phase transition of water or concurrently with water desorption from the surface.[22–24] Whilst smaller molecules generally exhibit trapping and release within the water ice, complex molecules are expected to give rise to more complicated behaviour. This is because COMs often have functional groups that can facilitate direct interactions with the water ice, as already reported for simple alcohols such as methanol and ethanol.[23,25–27]

a)Author to whom correspondence should be addressed. Electronic mail: darenburke@hotmail.com

Previously, Collings and co-workers classified the desorption behaviour of a wide range of small volatiles thought to be present within interstellar ices.[23] These classifications were subsequently used to model desorption on astrophysical time scales.[28,29] However, with the increasing detection of COMs in the ISM, it is now necessary to extend this classification to include larger, more complex molecules. With this in mind, we present a detailed temperature programmed desorption (TPD) and reflection absorption infrared spectroscopy (RAIRS) study of the interactions of the $C_2O_2H_4$ isomers, glycolaldehyde, methyl formate, and acetic acid, adsorbed on and within amorphous solid water (ASW) and crystalline water (CI) ices grown on highly oriented pyrolytic graphite (HOPG) at ~20 K. These isomers contain a range of functional groups that have varying strengths of intermolecular (within the pure ice) and intramolecular (with water) interactions.[8] As we show here, these interactions can influence the desorption behaviour of the isomers themselves, in addition to affecting the behaviour of the water ice.

Individual TPD and RAIR spectra have been briefly reported for all three pure isomers as an aid to identification during UV experiments studying the formation of various COMs.[14] We have previously studied the growth modes and temperature induced phase changes of all three pure isomers adsorbed on a graphitic substrate as a function of coverage.[8] These data are reported in detail elsewhere. However, we will give a brief summary of the results here. As a consequence of its very weak intermolecular interactions, methyl formate desorbs from graphite at the lowest temperatures (~115 K). Conversely, glycolaldehyde and acetic acid form hydrogen bonded moieties, resulting in higher desorption temperatures of ~140 and ~160 K, respectively. The hydrogen bonding in glycolaldehyde and acetic acid gives rise to zeroth order desorption from HOPG regardless of coverage, as also observed for methanol and ethanol desorption from graphene.[30]

To date, there are no previous studies reporting the interactions with and desorption of glycolaldehyde from water ices. However, the destruction of glycolaldehyde and mixed glycolaldehyde:water ices by proton irradiation has been studied by Hudson and Moore.[31] Similarly, there are a very limited number of studies investigating methyl formate interactions with water ice surfaces, with a majority of the work focusing on thermal processing on metallic surfaces.[32–34] Bertin and co-workers presented a study of methyl formate and acetic acid adsorption and desorption from ASW and CI films that combined experiment and theory.[6,35] This study focused on the interaction of submonolayer films with water ices using TPD and RAIRS at 80 K. The only studies at lower temperatures (16 K) have focused on the formation of methyl formate via the ion irradiation of methanol and CO ices.[12,13]

In contrast to glycolaldehyde and methyl formate, studies of acetic acid on water surfaces ≥80 K are more widespread, due to its relevance in atmospheric chemistry and catalysis. In addition to Bertin's study of acetic acid on CI,[6,35] its adsorption and desorption from water ice surfaces has been characterized by several groups. Gao and Leung studied the adsorption and desorption of acetic acid on amorphous and crystalline ice films using infrared spectroscopy in the temperature range of 123-180 K.[36] Bahr and co-workers conducted a detailed study of acetic acid adsorbed on ASW at 80 K using a combination of metastable impact electron spectroscopy, ultraviolet photoelectron spectroscopy, TPD, infrared measurements, and density functional theory (DFT) to explore the interactions between the two ices.[37,38] Hellebust *et al.* also studied acetic acid interactions with ASW as part of a wider study focusing on formic acid adsorption on water ice at liquid nitrogen temperatures.[39] The only study performed at very low temperatures (15 K) investigated the glass transition and morphology of acetic acid and its interaction with D_2O using time-of-flight secondary ion mass spectroscopy and TPD.[40]

This paper undertakes a comparative investigation of the adsorption, trapping, and desorption of glycolaldehyde, methyl formate, and acetic acid adsorbed on both ASW and CI and when co-deposited as a mixture with water at 20 K. TPD and RAIRS are used as a probe of the interactions between the water and the isomers. This is the first time that a detailed comparative study between the three isomers, under the same conditions, has been presented at temperatures which are relevant to astrophysical processes (20 K). Specifically, the thermal desorption of glycolaldehyde and water is examined for the first time. Furthermore, for all of the isomers our detailed coverage and composition dependent (with respect to mixed ices) studies of the full range of water containing ices allows us to accurately assign the desorption features and to carefully compare the behaviour of the three isomers. This in turn allows us to examine the adsorption and trapping of COMs at low temperatures, where the presence of high and low density forms of amorphous ice is significant with respect to the porosity and trapping ability of water ices.[41] We also examine the effects that the isomers have on the water desorption and crystallisation behaviour. Finally, we are able to extend the results obtained for these three isomers to provide a strong basis to categorize the desorption of these COMs based on the strength of intermolecular and intramolecular interactions as well as their desorption temperature. To validate our classifications, we also present TPD data for a variety of additional C, H, and O containing COMs. Our results demonstrate that the strength of intermolecular interaction is crucial in governing the desorption behaviour of a COM in the presence of water ice. Furthermore, we also show that the natural sublimation temperature of the COM with respect to water plays an important role in dictating the desorption of the water ice.

II. EXPERIMENTAL

TPD and RAIRS experiments were performed in two separate stainless steel ultra-high vacuum (UHV) chambers. Each chamber operated with a working pressure $\leq 2 \times 10^{-10}$ mbar. HOPG was used as a model carbonaceous dust grain analogue in both chambers. Samples were purchased from Goodfellows and cleaved prior to installation in the chamber by the Scotch tape method.[42] Samples were cleaned in UHV by cyclic annealing to 500 K, with substrate cleanliness confirmed by the absence of desorption products during TPD experiments performed without prior exposure. Both chambers were equipped with a closed-cycle helium refrigerator (SHI-APD), enabling cooling of the HOPG samples to base temperatures of 23 and

20 K for the TPD and RAIRS chambers, respectively. Temperature measurement and control were achieved via a Eurotherm 2048 control interface coupled to an E-type (TPD) or N-type (RAIRS) thermocouple.

Methyl formate (Sigma Aldrich, 99% anhydrous), acetic acid (Sigma Aldrich, ≥99%), and deionised water were purified by repeated freeze-pump-thaw cycles prior to deposition onto the HOPG surface. Solid glycolaldehyde dimer (Sigma Aldrich) was placed in a custom-built stainless steel vessel and pumped under vacuum ($p < 10^{-3}$ mbar) for several hours prior to heating to 95 °C until a constant pressure in the gas line was achieved. To remove residual amounts of water and further impurities from the heated glycolaldehyde sample, the dosing assembly was pumped again prior to dosing. To prevent the condensation of solid glycolaldehyde onto the walls of the dosing line, the entire assembly was maintained at a temperature of 95 °C throughout dosing. This method permitted the dosing of pure monomer glycolaldehyde onto the HOPG sample. The purity of all deposited ices was determined by mass spectrometry.

In both UHV chambers, ices were grown *in situ* by background dosing via high precision leak valves. Gas doses are given in Langmuir (L_m), where 1 $L_m = 1 \times 10^{-6}$ mbar s. Ices were grown either by sequential deposition from two separate leak valves (for layered ices) or by simultaneous deposition from two leak valves (for the ice mixtures). For ASW layered ices, typically 50 L_m (TPD) or 100 L_m (RAIRS) of water was deposited onto the surface at ~20 K prior to $C_2O_2H_4$ deposition. To ensure similar water ice morphologies across all ASW experiments, identical dosing pressures and geometries were used. Underlying crystalline water ices were grown by deposition of water ice onto a HOPG surface held at 130 K. In this case, the water exposures were adjusted to compensate for the decreased sticking probability of water on the HOPG surface at this temperature, thereby ensuring the growth of a crystalline ice with a thickness similar to that of the ASW ices. Following crystalline ice growth, the sample was cooled to base temperature prior to $C_2O_2H_4$ deposition. The crystalline structure of the water ices was confirmed by RAIRS. The composition of the co-deposited ices was determined by mass spectrometry in the vapour phase during exposure. In all cases, the amount of water ice remained constant and the differing compositions were obtained by varying the isomer concentration. Isomer concentrations varied between 5% and 50% depending on the experiment and isomer studied. The percentage of $C_2O_2H_4$ in the ice mixtures was determined by integrating the area under the resulting dose curves and correcting for mass spectrometer sensitivities to each species.

RAIRS data were recorded using a Thermo-Nicolet 6700 Fourier transform infrared spectrometer coupled to a liquid nitrogen cooled mercury cadmium telluride detector. All spectra were recorded at a resolution of 4 cm^{-1} and are the result of the co-addition of 256 scans. For the RAIRS annealing experiments, the sample was raised to the target temperature, held for 3 min, and then allowed to cool prior to recording a spectrum. All TPD spectra were recorded using a Hiden Analytical HAL 301/PIC quadrupole mass spectrometer in line-of-sight mode and differentially pumped. A range of masses was recorded for each species and each exhibited identical behaviour. Hence, the most intense mass fragment is shown in each case: mass 31 for methyl formate and glycolaldehyde and mass 43 for acetic acid. All TPD spectra were recorded with a linear heating rate of 0.5 K s^{-1}.

III. RESULTS AND DISCUSSION

A range of ice compositions were investigated with TPD and RAIRS. Data reported for TPD investigations are summarized in Table I, along with the observed peak temperatures in each case.

A. Methyl formate

1. TPD

Figure 1 shows TPD spectra for various configurations of binary ices containing methyl formate and water. These spectra

TABLE I. Summary of TPD experiments detailing ice compositions and desorption temperatures for acetic acid, glycolaldehyde, and methyl formate for all three water-ice configurations. (V) and (C) denote volcano and co-desorption peaks, respectively. Given peak temperatures are approximate due to coverage dependence of the TPD peaks.

	Acetic acid		Glycolaldehyde		Methyl formate	
	Composition	Peak temperature (K)	Composition	Peak temperature (K)	Composition	Peak temperature (K)
On 50 L_m ASW	1-50 L_m	150 160 172	1-20 L_m	161	1-20 L_m	114 118 127 145(V) 158(C)
On 50 L_m CI	0.5-10 L_m	161	0.5-10 L_m	161	0.1-5 L_m	118 129
Mixed ices (50 L_m of ASW)	8%-39%	159(C) 170	6%-20%	147(V) 161(C)	5%-24%	126 146(V) 160(C)

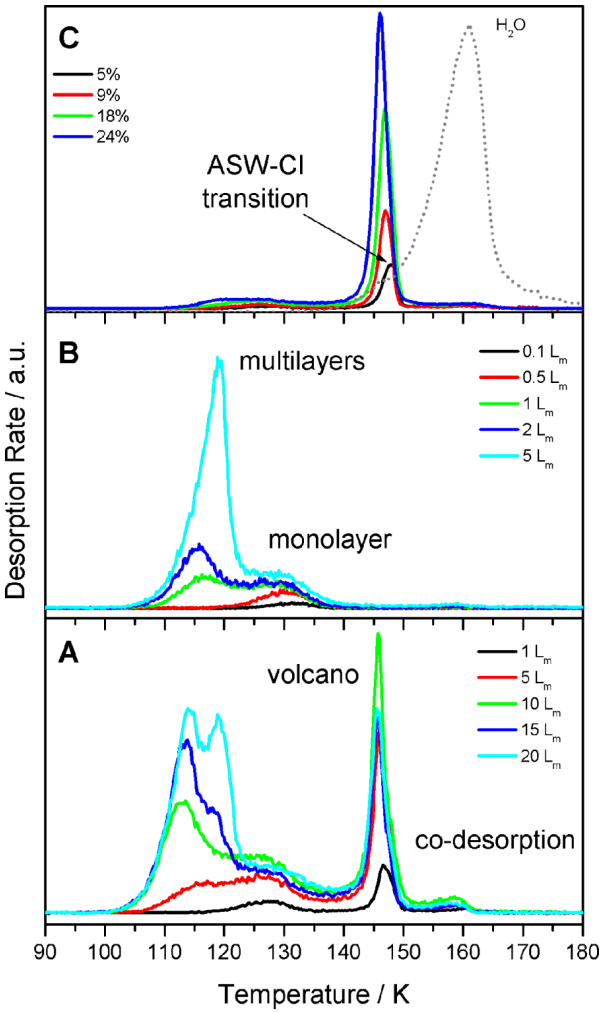

FIG. 1. Methyl formate TPD spectra following various exposures adsorbed on 50 L_m of (a) ASW, (b) CI, and (c) from co-deposited mixed ices adsorbed on HOPG at 23 K. Exposures of the overlayers ((a) and (b)) and the composition of the mixed ice with respect to methyl formate (c) are given in the figure. A scaled water TPD spectrum is shown in panel (c) to aid with the assignment of the methyl formate desorption peaks.

are in good agreement with those previously reported by Bertin *et al.* which were measured at liquid nitrogen temperatures (~80 K).[6] It is evident that there are four different modes of methyl formate desorption across the three ice configurations. The two high temperature desorption peaks observed in the ASW layered ice (Figure 1(a)) and mixed ice (Figure 1(c)) can be assigned by comparison with water desorption in each case (Figure 1(c)). The peak corresponding to the kink on the leading edge of the water desorption (~145 K) is assigned to the release of methyl formate trapped within the pores of the ASW ice structure during the amorphous to crystalline phase transition. This so called volcano peak[43] has been readily observed for a variety of smaller volatiles adsorbed in the presence of water ice.[22–24,44] For the mixed ices, the volcano desorption mechanism clearly dominates the desorption across the range of percentages studied. Similarly, when methyl formate is deposited beneath a 50 L_m ASW layer (not shown), a very sharp volcano peak is also observed. Clearly, despite its size, methyl formate behaves in the same way as smaller volatiles.

The smaller desorption peak at higher temperature (~160 K), which is coincident with bulk water desorption, is assigned to co-desorption of methyl formate with CI. This desorption component is the minor feature for both the layered and mixed ices. This co-desorption feature was not observed previously for ice grown at higher temperatures.[6] The appearance of a co-desorption feature in this work is most likely due to the lower deposition temperature used here (23 K), which gives rise to water ice with higher porosity than that grown at higher temperatures.[41]

The lower temperature desorption peaks observed between 110 and 130 K for both ASW and CI layered ices (Figures 1(a) and 1(b)) can be assigned by comparison with the desorption of methyl formate from a bare HOPG surface.[8] Pure methyl formate adsorbed on HOPG shows a monolayer desorption peak at ~104 K and multilayer desorption at temperatures >110 K. On both layered water ices, methyl formate TPD spectra initially show the growth of a single desorption peak at ~127 K. This peak saturates with increasing exposure and is assigned to the desorption of methyl formate monolayers bound directly to the water surface. This peak occurs ~20 K higher compared to the equivalent monolayer peak observed on HOPG.[8] This higher desorption temperature suggests a stronger interaction between methyl formate and water ice compared to that between methyl formate and HOPG. The nature of the interaction between methyl formate and water can be inferred by comparison with adsorption on metallic surfaces and with DFT calculations on water ice surfaces. RAIRS studies of the adsorption of methyl formate on Ag{111}[32] and Ni{111}[33] have shown that the molecule adopts a structure where the carbonyl group is oriented towards the substrate, forming a strongly physisorbed or weakly chemisorbed structure. DFT calculations for methyl formate adsorption on water ice also show that methyl formate interacts with the surface via the carbonyl group.[35] We suggest that this same structure gives rise to the more strongly bound physisorbed species observed for methyl formate adsorbed on ASW and CI. A similar assignment was also proposed by Bertin *et al.*[6] This stronger interaction with the water ice surface is supported by a preliminary desorption energy determination for (sub)monolayer methyl formate on both CI and ASW ices. Analysis of the data shown in Figures 1(a) and 1(b) gives desorption energies of 38.4 ± 4.4 and 36.7 ± 4.4 kJ mol^{-1} for CI and ASW, respectively. These values are in agreement with those reported previously[6,35] and are somewhat higher than those determined for submonolayer exposures of methyl formate on bare HOPG (18.1 ± 1.2 kJ mol^{-1}).[8]

Finally, the low temperature peak observed for methyl formate adsorption on both ASW and CI layered ices is assigned to the formation of methyl formate bilayers and multilayers at higher coverage (not shown) which are also observed for pure ices adsorbed on HOPG.[8] This assignment differs from that of Bertin *et al.*, who assigned the bilayer peak to a crystalline form of methyl formate formed during the heating process.[6] However, as shown by the RAIRS data discussed below, methyl formate does not undergo a phase transition when adsorbed on ASW and hence this peak cannot arise due to the desorption of crystalline methyl formate.

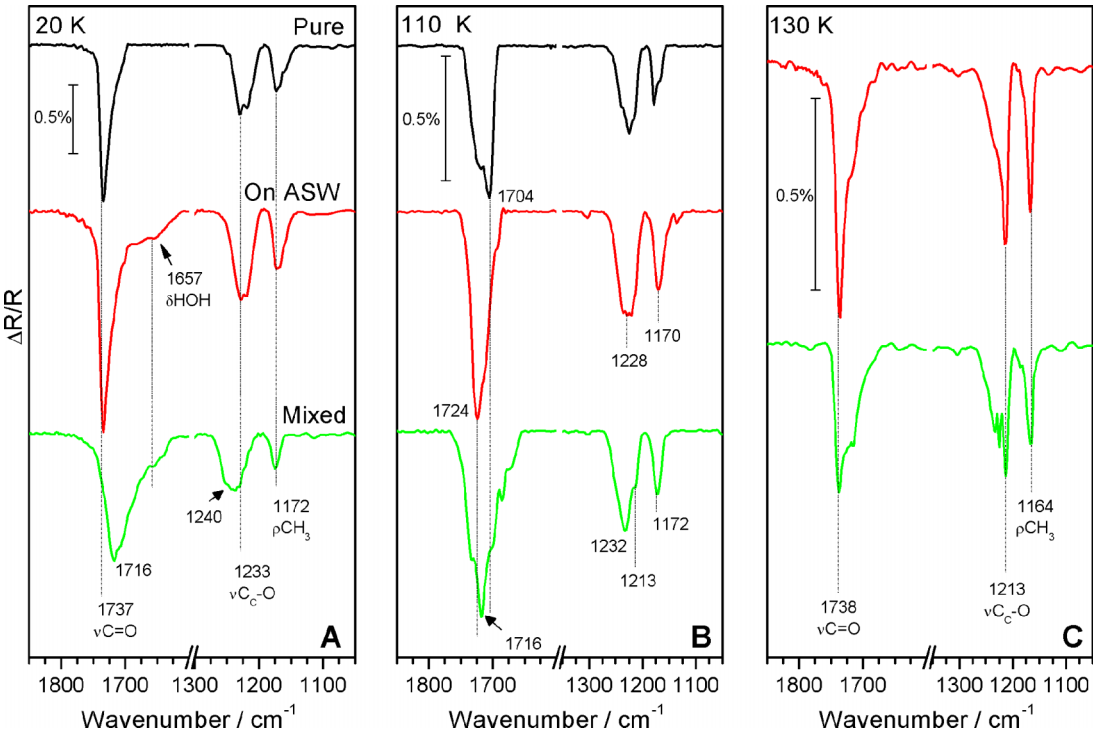

FIG. 2. RAIR spectra focusing on the 1850–1050 cm^{-1} region for a 40 L_m layered methyl formate/water ice (red traces) and a 27% co-deposited methyl formate:water ice (green traces) adsorbed on HOPG at 20 K and annealed to different temperatures. (a) shows the traces upon adsorption at 20 K. Panels (b) and (c) show the ices annealed to 110 and 130 K, respectively. Panels (a) and (b) include a spectrum for a 40 L_m pure methyl formate ice (black traces) for comparison. Band intensities are different for each temperature and are included in the figure. Symbols: ρ, rocking mode, ν, stretching mode, and δ, bending mode.

2. RAIRS

Figure 2 shows RAIR spectra comparing the thermal evolution of pure, layered (ASW) and co-deposited methyl formate:water mixed ices. The figure focuses on the C═O and C_C—O regions of the infrared spectrum, since these infrared bands are key indicators of the phase of the methyl formate ice and illustrate the interactions of methyl formate with water.

For the water containing ices, the RAIR spectra for methyl formate recorded at 20 K (Figure 2(a)) compare well with those of pure methyl formate ice, exhibiting all of the infrared bands observed in the pure ice.[8] The binary layered ice spectrum shows a strong resemblance to that of the pure methyl formate ice, which is unsurprising since methyl formate forms physisorbed multilayers on ASW in the same way as on HOPG. The main difference between the RAIR spectra of the pure and water containing ices is a low wavenumber shoulder on the C═O band centred around 1657 cm^{-1}, which is observed in the water containing ices (Figure 2(a)). This is assigned to the HOH scissors mode of ASW[45,46] and is also clearly visible in the layered and mixed glycolaldehyde:water ices (shown later). The methyl formate:water mixed ice also shows some subtle differences when compared to the layered and pure ices (Figure 2(a)). Both the C═O and C_C—O bands are broader when compared to those seen for the pure ice and are shifted to 1716 cm^{-1} and 1240 cm^{-1}, respectively. The shift in the C═O band can be assigned to an interaction between the methyl formate molecules and the ASW. A similar red-shift was observed when methyl formate was adsorbed on metallic surfaces[32,33] and is consistent with the additional desorption peak which is observed in the methyl formate TPD spectra on both ASW and CI films, assigned to the desorption of methyl formate bonded directly to water (Figures 1(a) and 1(b)).

Following annealing to 110 K (Figure 2(b)), the pure ice undergoes a structural ordering leading to changes in the infrared spectrum, including band splitting, spectral shifts, and changes in band intensity, as described previously.[8] These spectral modifications are not observed for either of the water containing ices. Rather, the methyl formate C═O band for the layered ASW ice broadens and red-shifts ~13 cm^{-1} to 1724 cm^{-1}, while the C_C—O (1228 cm^{-1}) and CH_3 (1170 cm^{-1}) bands do not exhibit the splitting or change in band profile that is observed for the pure ice. Clearly the underlying ASW layer inhibits the thermally induced restructuring of the methyl formate overlayer. At the same annealing temperature, the mixed ice spectrum shows a narrowing of the C═O band, but without a corresponding spectral shift. In addition, the C_C—O band exhibits a blue-shift of ~8 cm^{-1}.

The similarity between the layered and mixed ice spectra at 110 K suggests thermally induced mixing between the methyl formate and water layers has occurred when the layered ice is annealed. Further heating to 130 K (Figure 2(c)) results in very similar spectra for the binary layered and mixed ices, with the C═O band for both ices blue-shifting to 1738 cm^{-1} in addition to the C_C—O (1213 cm^{-1}) and CH_3 (1164 cm^{-1}) bands showing strong similarities for the two ice configurations. The spectra in Figure 2(c) must be the vibrational signature of methyl formate trapped in the water ice since the surface species has already desorbed by this temperature. This is in agreement with the methyl formate TPD spectra (Figure 1)

which show the desorption of trapped methyl formate at the ASW-CI phase transition at ~145 K.

Clearly, both TPD (Figure 1) and RAIRS (Figure 2) data show that thermally induced mixing occurs between the methyl formate overlayer and the underlying water surface. The extent of the mixing is not complete when compared to a co-deposited ice, as evidenced by the presence of surface desorption of methyl formate at its natural sublimation temperature in the TPD (Figure 1(a)). However, it is enough to inhibit the re-structuring of the methyl formate film. Similar effects have been observed for ethanol/ASW layered ices adsorbed on HOPG at 98 K.[26]

Our assignment of the C=O spectral shift to thermally induced mixing is at odds with Bertin *et al.*, who ascribed a similar red-shift to a structural change in the methyl formate film.[6] Clearly, our pure methyl formate and layered ices do not show the same RAIR spectra following annealing to 110 K. The differences between our spectra and those of Bertin could arise from the different temperatures at which the water ices are grown in the two studies. Deposition temperatures of 20 K are known to give rise to ASW with a lower density and greater porosity compared to ice growth at 80 K.[41] Hence, our ices contain less pure methyl formate and more methyl formate that is adsorbed in the pores of the water ice when compared to Bertin's data. This is confirmed by a comparison of the ratios between the monolayer and volcano peaks observed in our methyl formate TPD spectra (Figure 1) and those of Bertin.[6] Our data show a much larger volcano component, confirming this assertion. Hence, the extent of the thermally induced mixing in our experiments is greater compared to those reported by Bertin and hence we do not observe a structural change for methyl formate adsorbed on ASW.

B. Acetic acid

1. TPD

Figure 3 shows TPD spectra for low exposures of acetic acid adsorbed on ASW (Figure 3(a)) and CI surfaces (Figure 3(b)). Data for higher acetic acid exposures on ASW, and also for co-deposited mixed ices are shown in Figure 4. Our data are in broad agreement with previous data, but with some important differences, particularly with respect to the assignments, where our detailed comparison of acetic acid adsorbed on ASW, CI, and in mixtures allows us to accurately assign the observed desorption peaks. Acetic acid desorption from CI (Figure 3(b)) is simple, giving rise to a single peak at ~160 K that desorbs concurrently with CI. In contrast, desorption from ASW is more complex, with three distinct peaks visible in the TPD spectrum. Assignment of these peaks can be made by comparison between the two systems and the existing literature. At the lowest exposures on ASW (1-2 L_m), a single acetic acid peak is observed which co-desorbs with bulk water (Figure 3(a)). Since this peak is the first to be observed, it is assigned to the desorption of monolayer acetic acid interacting directly with ASW. This is confirmed by an approximately constant desorption temperature with increasing exposure, coupled with non-shared leading edges in the TPD spectra. The formation of a monolayer is in agreement with previous TPD[6] and infrared studies[36] and is in contrast to

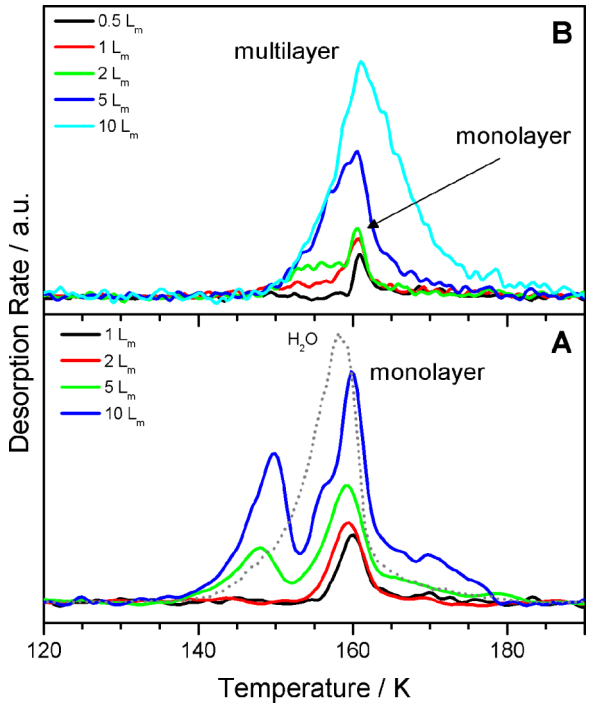

FIG. 3. TPD spectra for low exposures of acetic acid deposited on (a) 50 L_m ASW and (b) 50 L_m CI on HOPG at 23 K. The exposures are detailed in the figure. A scaled water TPD spectrum is shown in panel (a) (grey dotted line) to aid with the assignment of the acetic acid desorption peaks.

the adsorption of pure acetic acid on HOPG, where zero order desorption is observed irrespective of coverage.[8] Bahr *et al.* suggested that acetic acid adsorbs onto the water ice surface as cyclic dimers, forming two strong hydrogen bonds which have

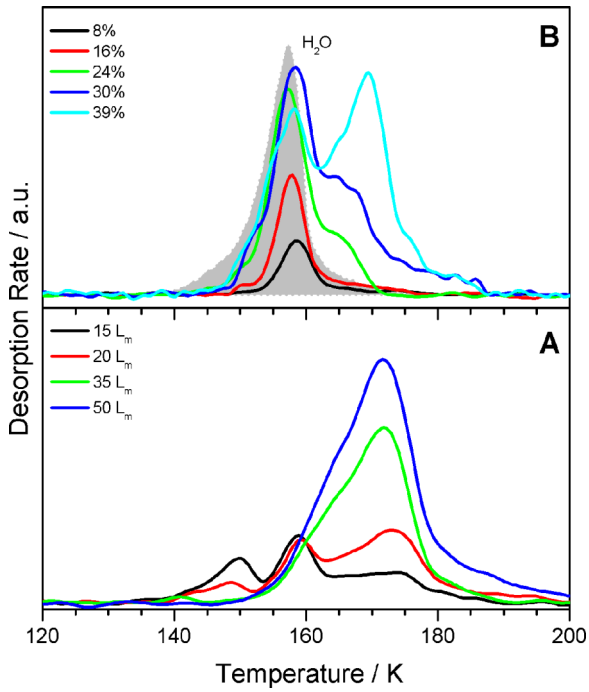

FIG. 4. (a) High exposures of acetic acid deposited on 50 L_m of ASW on HOPG at 23 K. (b) TPD spectra for co-deposited acetic acid and water mixed ices adsorbed on HOPG at 23 K. In both cases, the acetic acid percentages (with respect to water) or overlayer exposures are given in the figure. A scaled water TPD peak (gray shaded) is included with the mixed ices to illustrate the co-desorption and residue components of the acetic acid desorption.

equivalent interaction energies to those of water ice.[37] RAIR spectra (shown later) also indicate that the acetic acid initially adsorbs on the ASW surface at 20 K in the form of cyclic dimers, further confirming this assignment. The interaction between acetic acid and water gives rise to a slightly higher desorption temperature for acetic acid (~10 K higher) on ASW compared to the pure ice adsorbed on HOPG, in agreement with Souda.[40]

With increasing acetic acid exposure on ASW, a second lower temperature peak grows into the spectrum at 148 K (Figure 3(a)), which is visible for exposures between 5 and 10 L_m (extending up to 20 L_m in Figure 4(b)). This peak is not observed at equivalent (or higher) exposures on CI and therefore must be associated with the porous and heterogeneous nature of the ASW surface. It is therefore likely that this peak is due to acetic acid adsorbed within the ASW pores, where intermolecular interactions are dominated by neighbouring acetic acid molecules. The desorption temperature of this peak is similar, but not identical, to that observed for pure acetic acid ices at the lowest exposures, thus supporting this assignment.[8] A more definitive assignment of this peak can be made by reference to higher exposures of acetic acid adsorbed on ASW, shown in Figure 4(a), and is discussed later. For acetic acid exposures ≥10 L_m, a high temperature peak evolves at 169 K. This peak goes on to dominate the TPD spectrum with increasing exposure (Figure 4(a)) and will be discussed later with respect to the deposition of higher exposures of acetic acid.

Figure 3(b) shows the desorption of acetic acid from the surface of CI. By comparison to Figure 3(a), the single desorption peak at the lowest exposures (≤2 L_m) can be assigned to the desorption of monolayer acetic acid from the CI surface. Again, this assignment is confirmed by an almost constant desorption temperature and non-shared leading edges in the TPD. Increasing the acetic acid exposure sees the development of multilayer acetic acid on the CI surface (as evidenced by the appearance of a peak with shared leading edges), which grows in at lower coverages compared with those observed on ASW, as expected. This adsorption behaviour is due to differences in the porous and non-porous surfaces of the ASW and CI, respectively. Our TPD spectra for acetic acid on CI are at odds with those reported by Bertin *et al.* who observed the presence of three distinct peaks in their study of acetic acid adsorption on CI at 80 K.[6] These differences could be a consequence of the different heating rates; 1 K min^{-1} in their study compared to the faster rate of 0.5 K s^{-1} used here. However, the differences could also be as a result of the crystallinity of the underlying water film in the two experiments. Our acetic acid TPD spectra from ASW strongly resemble those obtained by Bertin for acetic acid desorption from CI.

Figure 4 shows the desorption of higher exposures (15-50 L_m) of acetic acid from ASW (Figure 4(a)). With increasing acetic acid exposure, it is clear that the monolayer saturates at an exposure of 15 L_m, whilst the high temperature peak visible at lower exposures (10 L_m) goes on to dominate the TPD spectrum. This high temperature peak is assigned to the desorption of multilayer acetic acid that has undergone a phase transition to form polycrystalline polymer chains.[37] Similar behaviour is also observed for high exposures of acetic acid adsorbed on CI surfaces (not shown). In both cases, the acetic acid desorbs at higher temperatures compared to the underlying water ice, showing that water is able to sublimate through the acetic acid film. The low temperature TPD peak (assigned to acetic acid adsorbed within the ASW pores) is also visible in the spectrum at 15 L_m. This peak clearly decreases in intensity with increasing acetic acid exposure, before completely disappearing from the spectrum by 35 L_m. The decreasing intensity of this peak directly correlates with the increase of the multilayer peak. This observation is ascribed to the acetic acid isolated in the pores of ASW becoming incorporated into the multilayer crystalline network during heating, an effect that is dependent on the thickness of the acetic acid overlayer.

Figure 4(b) shows the TPD spectra for co-deposited mixtures of acetic acid:water ices for various compositions ranging from 8% to 39%. TPD spectra for the mixed ices comprise of either one or two desorption features, dependent on the composition. For lower acetic acid percentages (≤20%), a single desorption peak is observed that is concurrent with water desorption. This is assigned to co-desorption of acetic acid and water. This simultaneous desorption has been observed previously in the TPD of mixed acetic acid:water ices[39] and has been ascribed to hydrogen bonding between acetic acid and water molecules or to the formation of a complex hydrate.[36,39] As the percentage of acetic acid in the water ice increases, an additional high temperature peak, which desorbs after the water has desorbed, grows into the spectrum. This residue, following acetic acid co-desorption, is assigned to a form of pure polycrystalline acetic acid (see RAIRS below). The presence of this residue of pure acetic acid suggests that thermally induced segregation occurs between the acetic acid and water at higher acetic acid ice compositions. The threshold for segregation is approximately 24%-40%, which is further confirmed by RAIRS later. Similar behaviour, where the bulk of acetic acid desorbs after complete desorption of the water ice film, is also observed for thicker layers of acetic acid adsorbed on water ice (Figure 4(a)) and has been reported previously.[6,36,37,39]

2. RAIRS

To gain further understanding of the nature of the acetic acid residue, RAIRS annealing experiments were performed for various layered and mixed ice configurations. Figure 5(a) compares the RAIR spectra for the layered and co-deposited acetic acid:water ices at 20 K. The figure focuses on the C═O and C—O region of the spectrum, since these bands are good indicators of the environment and the phase of the acetic acid ice.[36,37] The acetic acid spectrum resulting from the layered ice at 20 K is almost identical to that of pure acetic acid adsorbed on HOPG, with all the corresponding infrared bands present in the spectrum.[8] Only the infrared bands that are obscured by the presence of water are absent. The similarity between the acetic acid spectra on the two surfaces suggests that the overlayer consists of both monomers and dimers upon adsorption, as indicated by the carbonyl region of the spectrum which is a sensitive probe of both species.[36,37] The split C═O band at 1733 and 1718 cm^{-1} results from the presence of acetic acid dimers and the high wavenumber shoulder at 1760 cm^{-1} is assigned to monomers.[8,37]

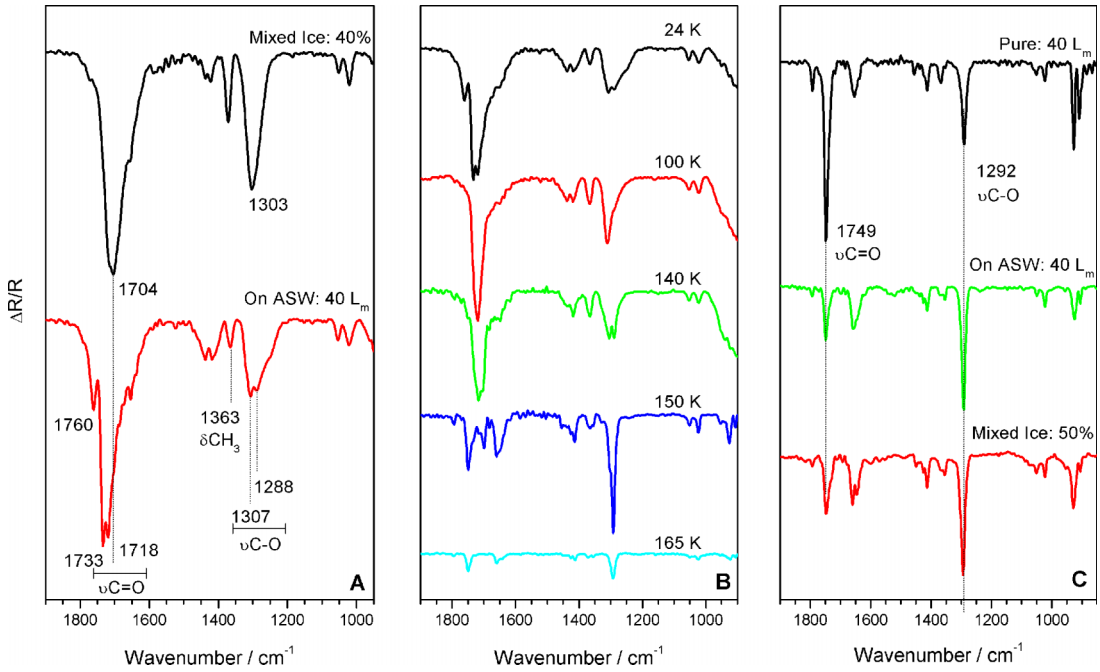

FIG. 5. RAIR spectra focusing on the C=O and C—O region for various ice configurations of acetic acid deposited on HOPG at 20 K. (a) Comparison of 40 L_m of acetic acid deposited on 100 L_m of ASW with a co-deposited 40% mixture of acetic acid:water at 20 K. (b) Annealing series of 40 L_m of acetic acid deposited on 100 L_m of ASW at selected temperatures. The temperature of each trace is outlined in the figure. (c) Comparison of 40 L_m of pure acetic acid, 40 L_m of acetic acid deposited on 100 L_m of ASW, and a 50% co-deposited acetic acid:water ice all annealed to 160 K. In each case where the water is present, the amount of water ice was identical (100 L_m). Symbols: ν, stretching mode and δ, bending mode.

In contrast to the layered ice, the mixed ice gives rise to broader infrared bands, some of which are also shifted. Specifically, the C=O band of the 40% mixed ice is red-shifted by 29 cm^{-1} to ~1704 cm^{-1} when compared to the layered ice. This shift is dependent on the composition of the mixed ice, with lower percentages of acetic acid giving rise to carbonyl bands with a larger red-shift (23%:1693 cm^{-1}). Hence, the shift in peak position is assigned to intermolecular interactions between the acetic acid and water. The broadening of the infrared bands in the mixed ice is most likely due to a combination of hydrogen bonding between the acetic acid and water molecules and the heterogeneity of the amorphous ice environment.[39]

Figure 5(b) shows RAIR spectra following annealing of the 40 L_m acetic acid film deposited on ASW at 20 K. Annealing the layered ice gives rise to very minor structural changes up to temperatures of 90 K (not shown). Continued heating up to 100 K leads to a restructuring of the ice, as clearly shown by the changes in the infrared spectrum. No further changes occur in the spectrum until 140 K, where the spectrum reverts back to a profile strongly resembling the infrared spectrum at 20 K. Further heating to 150 K leads to dramatic changes across the entire spectrum, coinciding with the loss of the water peaks (not shown). The resulting infrared spectrum can therefore be assigned to acetic acid that remains on the surface after water desorption from HOPG. This result is consistent with the observation of an acetic acid residue in the TPD (Figure 4(a)) that desorbs after the water ice.

In contrast to the layered ices, annealing the 50% acetic acid mixed ice (not shown) gives rise to very minor changes across the annealing range until the desorption of water at 150 K, at which point the infrared spectrum changes markedly. The resulting infrared spectrum is identical to that observed for the layered ice following annealing, as shown in Figure 5(c). By comparison with the TPD spectra (Figure 4), which shows an acetic acid peak that desorbs after water (for higher acetic acid overlayers and ice compositions), these infrared spectra can therefore be assigned to the signature of the residue that remains on the surface after the water has desorbed.

The nature of the residue from both the layered and mixed acetic acid:water ices can be determined by comparison with the infrared spectrum following the annealing of pure acetic acid ice to 160 K, which gives rise to crystalline ice. Figure 5(c) compares the infrared spectra of all three ices following annealing to 160 K. It is clear from Figure 5(c) that there is a strong resemblance between the spectra of the layered and mixed ice acetic acid residue and that of the pure crystalline ice. All of the spectral features observed for the pure crystalline ice are present in the spectra seen in Figure 5(c), however, it is noted that the peak due to the C—O band at 1292 cm^{-1} is the most intense for the residue ice, as opposed to the C=O peak at 1749 cm^{-1} which is the most intense for the pure crystalline ice. Due to the similarity of the spectra shown in Figure 5(c) with that of the crystalline acetic acid ice, we assign the residue to pure acetic acid which has crystallised at the point at which the water desorbs from the HOPG surface. It is not clear exactly what the form of the crystalline ice is, particularly given that the intensity ratios of the C—O and C=O bands are different for the pure and the residue ice. However, it is clear that the ice that remains following the water desorption is a highly ordered form of acetic acid.

There is a threshold for the observation of this residue of acetic acid that remains on the surface following the desorption of the water ice. The TPD spectra shown in Figure 4(b) indicate

that the residue is only observed following doses >15–20 L_m (Figure 4(b)) for layered ices and for acetic acid compositions >30% for the mixed ices. For the RAIR spectra, this residue is not observed for 20 L_m layers of acetic acid on ASW, but is seen for 40 L_m overlayers. For the co-deposited ices, this residue is only observed in the RAIR spectra following the annealing of ices containing more than 40% acetic acid with respect to water. The apparent anomaly between the TPD and RAIRS results is attributed to two factors. First, the increased sensitivity of TPD over RAIRS and second the minor variation in dosing between the TPD and RAIRS UHV chambers.

C. Glycolaldehyde

1. TPD

Figures 6(a) and 6(b) show TPD spectra of increasing exposures of glycolaldehyde adsorbed on pre-deposited ASW and CI, respectively. In contrast to methyl formate and acetic acid, glycolaldehyde desorption from both CI and ASW ice surfaces is simple and also gives rise to essentially identical behaviour.

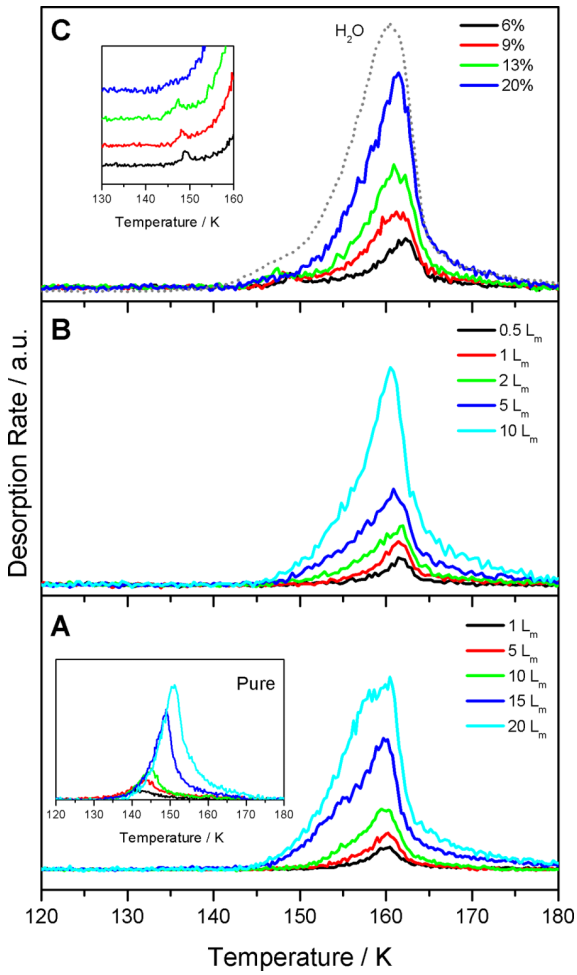

FIG. 6. TPD spectra for increasing exposures of glycolaldehyde deposited on an underlying 50 L_m ice of (a) ASW and (b) CI adsorbed on HOPG at 23 K. The inset in panel (a) shows the TPD for pure glycolaldehyde adsorbed on HOPG at 23 K for exposures ranging from 0.5 to 10 L_m. (c) shows TPD spectra for varying compositions of mixed glycolaldehyde:water ices adsorbed on HOPG at 23 K and includes a scaled 50 L_m water TPD trace for comparison. The inset to panel C highlights the volcano desorption peak for the lower concentrations. All glycolaldehyde exposures and concentrations with respect to water are given in the figure.

Glycolaldehyde desorption from ASW and CI exhibits a single TPD peak at ~160 K. This peak has a constant desorption temperature, and does not share leading edges, suggesting that glycolaldehyde forms monolayers on both water surfaces regardless of the ice morphology. This behaviour contrasts that observed for glycolaldehyde desorption from bare HOPG (Figure 6(a) inset), where only zeroth order desorption is observed irrespective of exposure. Furthermore, glycolaldehyde adsorbed directly on HOPG exhibits a distinctive phase change for exposures ≥30 L_m (assigned to crystallization by RAIR spectra).[8] However, there is no evidence of this change for the glycolaldehyde layered systems, up to exposures of 50 L_m (not shown). The different desorption behaviour of glycolaldehyde adsorbed on water ices compared to that adsorbed on HOPG provides evidence of an interaction between the glycolaldehyde and water ice surfaces. On HOPG, zeroth-order kinetics suggested that glycolaldehyde preferentially bonds to itself rather than HOPG.[8] However, on water ice surfaces, glycolaldehyde has the possibility to form hydrogen bonds to the surface and hence forms a monolayer upon adsorption. Further evidence of this interaction is provided by an upshift in the desorption temperature of low exposures of glycolaldehyde on water surfaces compared to on HOPG, which is clearly shown in Figure 6(a). It is also noted that the kinetics of glycolaldehyde desorption changes from zeroth order on HOPG to first order desorption when adsorbed on ASW and CI surfaces. This modified desorption behaviour is similar to that of acetic acid, which also exhibits an upshift in desorption temperature, in addition to the formation of monolayers on water ices at low exposures via the formation of hydrogen bonded moieties. However, in contrast to acetic acid, glycolaldehyde does not give rise to a residue remaining on the HOPG surface following the desorption of water even at higher glycolaldehyde exposures.

Figure 6(c) shows TPD resulting from a co-deposited mixture comprised of varying glycolaldehyde concentrations. At all concentrations, glycolaldehyde desorption is dominated by co-desorption with water, with a desorption profile that strongly resembles that of the two layered ices. This suggests either significant mixing occurs between the layers prior to desorption (unlikely for CI) or the strength of the intermolecular interactions between two glyocolaldehyde molecules and between glyocolaldehyde and water is equivalent. It is more likely that the interactions are equivalent in all ices, and this is confirmed by RAIRS later.

For glycolaldehyde concentrations <19%, there is also a very small peak at ~148 K (Figure 6(c) inset). This peak is coincident with the phase change observed for ASW and is therefore assigned to volcano desorption of glycolaldehyde. The appearance of a volcano component for the glycolaldehyde mixtures and not for the layers is most likely a consequence of complete mixing for the co-deposited ices upon deposition, compared to the thermally induced mixing in the layers. The reduction and eventual loss of the volcano component for the mixed ices with increasing glycolaldehyde composition is probably a result

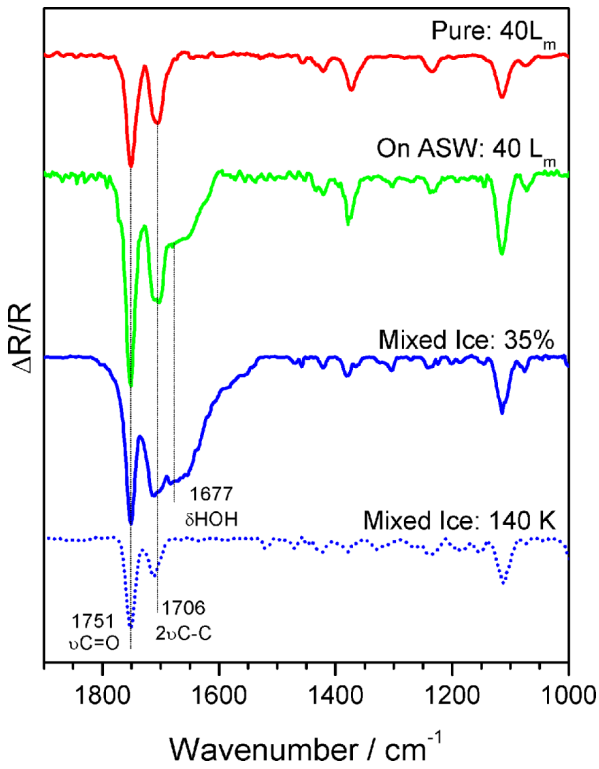

FIG. 7. RAIRS of various ice configurations of glycolaldehyde deposited on HOPG at 20 K showing the spectral region between 1850 and 1000 cm^{-1}. The bottom trace (dotted line) shows the resulting RAIR spectra for a 35% glycolaldehyde:water mixed ice annealed to 140 K. Symbols: ν, stretching mode and δ, bending mode.

of the inhibiting effect of glycolaldehyde on the crystallization of ASW.

2. RAIRS

Figure 7 (top three traces) shows a comparison of the RAIR spectra of pure, layered and mixed (35%) glycolaldehyde:water ices adsorbed on HOPG at 20 K.

The infrared bands assigned to glycolaldehyde are very similar for the three ice configurations. All bands observed in the pure glycolaldehyde ice are present in the layered and mixed ices, with the exception of those masked by the presence of the water.[8] Hence, the infrared band assignments previously given for the pure glycolaldehyde ice are also valid for both layered and mixed ices. At first glance, the band at ~1706 cm^{-1}, assigned to the overtone of the C—C mode (enhanced via Fermi resonance), broadens with the presence of water. This effect is more obvious in the mixed ices. However, on closer inspection it is clear that the original overtone band from the glycolaldehyde is superimposed onto the water scissors mode at ~1677 cm^{-1}.[45] Across the rest of the spectrum, there are some subtle changes in the position of the infrared bands, with minor spectral shifts observed in the C—H region around 3000-2700 cm^{-1} (not shown). Importantly, the C═O stretch at 1751 cm^{-1} remains unchanged in all three ice configurations.

Annealing the layered and mixed ices shows very little change in the RAIR spectra recorded as a function of annealing temperature, as shown in Figure 7 (bottom trace) for the 35% mixed ice annealed to 140 K. This is in contrast to the annealing of pure glycolaldehyde ice which shows changes in the RAIR spectra upon annealing to 140 K, assigned to the crystallization of the glycolaldehyde ice.[8] The absence of glycolaldehyde crystallization for the water containing ices is not due to the differing amounts of glycolaldehyde ice present in the different ice configurations, as mixtures comprised of various compositions exhibit the same effects. Hence, the inhibited crystallization effect is assigned to the presence of the water ice. In fact, the infrared bands assigned to glycolaldehyde do not show any discernible spectral shifts during the annealing process and simply disappear when the water desorbs at 150 K, in agreement with the TPD (Figure 6). The only clearly observable spectral change in the glycolaldehyde RAIR spectra is the disappearance of the OH scissors mode, which has disappeared from the spectrum by 70 K.

The similarity between the pure glycolaldehyde and the water containing glycolaldehyde ices during adsorption, and the lack of crystallization for glycolaldehyde in the water containing ices, indicates that either glycolaldehyde does not interact with the water ice, or alternatively the nature of the glycolaldehyde-water interactions are equivalent to those between glycolaldehyde molecules. Evidence of an interaction between glycolaldehyde and water is given by the TPD spectra, which clearly show an upshift in desorption temperature coupled with the different growth mode of glycolaldehyde on water compared to bare HOPG. Hence, the interactions between glycolaldehyde and water must be similar in nature to the intermolecular interactions between glycolaldehyde molecules.

D. Isomer effects on water desorption and crystallization

Water is the dominant component of interstellar ices, hence its behaviour governs the trapping and release of other interstellar ice constituents. Studies that investigate the adsorption of various species on and in water ice usually focus on the effect that water has on the adsorbate, and the effect that the adsorbate itself has on the water is often overlooked. However, given the importance of water ice in dictating the behaviour of other adsorbed (and trapped) species, it is important to understand how these interactions change the properties of the water ice itself.

Many laboratory studies have shown that smaller non-interacting species, such as CO_2 and CO, do not directly affect the desorption of the dominant water component of the ice.[23,47] However, molecules that exhibit hydrogen bonding, such as methanol or ethanol, can directly affect the water ice. First, the water TPD desorption profile may be modified by the presence of a guest molecule in the water matrix, as observed for methanol,[25] ethanol,[26] and glycine.[48,49] Second, the crystallization of ASW may also be modified by interactions of an impurity, e.g., methanol, which lowers the temperature of the onset of crystallization[27] and hence modifies the desorption of trapped molecules.[50] As already shown above, the three $C_2O_2H_4$ isomers have a varying strength of interaction with water, and hence it is expected that they will

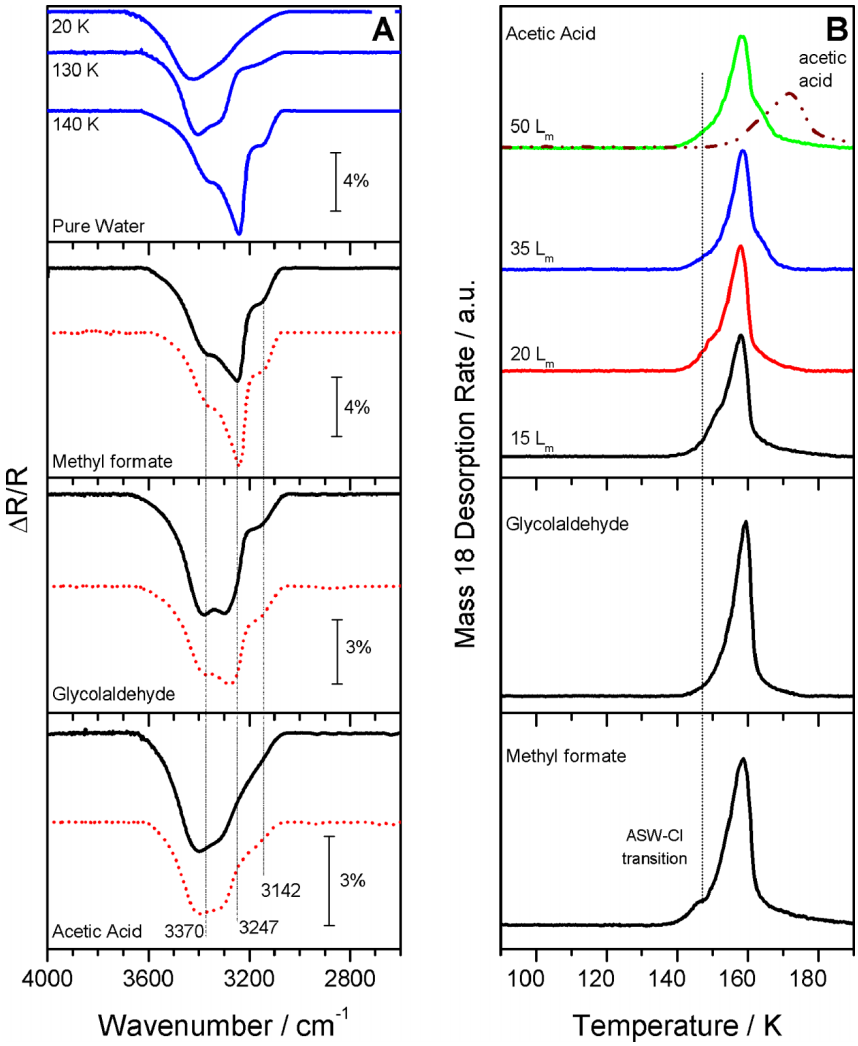

FIG. 8. (a) RAIR spectra showing the changes to the 4000–2600 cm^{-1} spectral region following the annealing of $C_2O_2H_4$ binary layered (red dotted lines) and co-deposited ices (black solid lines) to 140 K. In each case, the isomer overlayer was 40 L_m. Ice compositions (with respect to water) were 27%, 35%, and 40% for methyl formate, glycolaldehyde, and acetic acid, respectively. The top panel shows RAIR spectra for pure water ice at 20, 130, and 140 K for comparison. (b) Water TPD spectra for various $C_2O_2H_4$ overlayers. The top panel shows the water TPD for increasing acetic exposures. A scaled 50 L_m acetic acid trace is included to illustrate the origin of the high temperature shoulder on the water TPD. The lower panels show water TPD spectra following 15 L_m exposures of glycolaldehyde and methyl formate.

have differing effects on the desorption and crystallization of the water ice.

Figure 8(a) shows RAIR spectra for the OH stretch region following annealing to 140 K for the layered and mixed ices for all three isomers. This region of the spectrum provides a distinctive fingerprint that clearly distinguishes the ASW and CI phases of water.[45,51,52] A temperature of 140 K was selected for each ice since this temperature consistently shows the onset of any significant changes in the OH band of the spectrum. Pure water traces obtained for ASW (20 K) and CI (140 K), in addition to an intermediate transitional stage at 130 K, are included for comparison.

Comparing the water infrared traces obtained from the methyl formate layers and mixtures to that of pure CI at 140 K clearly shows that water crystallises in both cases. The layered methyl formate/water ice configuration exhibits a slightly greater extent of water crystallization compared to the methyl formate:water mixture. Furthermore, the water TPD trace obtained from the 15 L_m methyl formate layered ice (Figure 8(b)) clearly shows the distinctive kink on the leading edge of the water TPD which signifies the phase transition, indicating similar behaviour to that observed for pure water ice.[43] Identical TPD spectra were obtained irrespective of the methyl formate overlayer exposure (≤50 L_m). The same effects were also observed for the mixed ices regardless of composition (≤25%). Hence, both RAIRS and TPD show that methyl formate does not affect the thermal processing of water ice and in fact it behaves essentially as a small volatile with respect to water. Similar behaviour has also been reported for large non-polar molecules such as CCl_4,[43] n-hexane,[53] and decane,[27] in addition to polar molecules such as OCS,[44,50] as well as acetone and dimethyl ether (discussed later). This effect arises because the lower desorption temperature of methyl formate, coupled with its weak interaction with the water, does not inhibit the crystallization or desorption of the water ice.

In contrast, acetic acid has an obvious affect on the water ice upon annealing. The RAIR spectra for acetic acid layers and mixtures (Figure 8(a)) do not show any evidence for formation of CI following the annealing of mixtures or layers to 140 K, as shown by the OH band retaining the broad and featureless character of the ASW profile. This is consistent with the infrared study of Gao and Leung.[36] Clearly, the presence of acetic acid (either deposited on top of ASW or as a mixture) inhibits the formation of CI. Thermally induced intermixing of acetic acid-D_2O binary films above 130-140 K has been reported by Souda.[40] There is some evidence of thermally induced mixing in our RAIR spectra (Figure 5(b)) which

show that the annealed layered infrared spectrum at 140 K has similar features to those seen for the acetic acid:water co-deposited ice at 20 K (Figure 5(a)). Furthermore, the RAIR spectra for the annealed acetic acid/water layer shown in Figure 5(b) do not exhibit the trends observed for the pure acetic acid ice.[8] Although the extent of the thermally inducing mixing between the acetic acid and water layers is not complete, clearly the intermixing of the water and acetic acid that does occur disrupts the formation of the water crystalline network. As a result, acetic acid does not exhibit a desorption component at the amorphous to crystalline phase transition for layered or mixed ices.

The effect of adsorbed layers of acetic acid on the water TPD spectra is more complex compared to that observed in the infrared spectra. The TPD spectra (Figure 8(b)) clearly show an effect of increasing thickness of acetic acid on water desorption. For lower acetic acid exposures ($\leq$15 L_m) on ASW, the water TPD traces show evidence of a phase transition (not shown), however, the temperature at which this occurs shifts to higher temperatures compared to the water traces recorded for methyl formate layered ices. With increasing acetic acid overlayer exposure, the ASW-CI phase transition disappears from the spectrum by 35 L_m. In addition, a high temperature shoulder appears on the water TPD at 20 L_m, becoming more prominent following a 50 L_m acetic acid exposure. Bahr *et al.* reported the absence of the phase transition on the leading edge of the water TPD trace for their acetic acid adsorbed on ASW at 80 K and their results are consistent with our findings for higher exposures.[37] A high temperature shoulder develops on the water TPD for 35 and 50 L_m acetic acid overlayers. This shoulder is concurrent with the onset of acetic acid desorption (Figure 8(b)) and becomes more prominent with increasing overlayer exposure and therefore is not a simple case of delayed water desorption caused by the acetic acid overlayer that desorbs at higher temperature. This high temperature shoulder can be assigned to the co-desorption of acetic acid-water clusters which result from the strong interaction between acetic acid and water. Previous studies have reported an acetic acid–water co-desorption feature, however, this feature follows the natural water sublimation temperature, rather than giving rise to a delayed shoulder in the water TPD as observed here.[37] It is not clear why a high temperature shoulder is observed on our water TPD, when it was not observed previously. However, we note that our water dosing temperature is much lower at 20 K, which leads to the formation of a more porous water ice. We also note the different heating rate in our TPD experiment (0.5 K s^{-1}) compared to 1 K s^{-1} in previous studies.[37] It is possible that these combined factors could lead to subtle differences in the water TPD spectra in the two cases.

For acetic acid:water mixtures (not shown), the water TPD remains essentially unchanged with increasing acetic acid composition. There is no evidence of the ASW-CI phase transition on the leading edge of the water TPD peak and no high temperature shoulder is observed (Figure 4(a)). This is most likely due to the more complete mixing for the co-deposited ices compared with the limited thermally induced mixing that occurs between the binary layered ices. This is confirmed by the RAIR spectra shown in Figure 8(a), which consistently show (for all three isomers) that a mixed ice configuration inhibits the crystallization of water to a great degree compared to the layered ices.

The water RAIRS traces obtained from the glycolaldehyde layers and mixtures (Figure 8(a)) show an intermediate effect of glycolaldehyde on the water crystallisation. In this case, the profile of the OH infrared band has changed, showing partial transformation from ASW to CI. This is illustrated by the shifting of the OH band intensity to the lower wavenumber side of the band and the development of a low wavenumber shoulder at ~3150 cm^{-1}, both of which correspond to the formation of CI.[45,51] The TPD spectrum (Figure 8(b)) also shows that glycolaldehyde has an effect on the crystallization of ASW. The water TPD spectrum in this case shows little evidence of the characteristic phase transition from ASW to CI,[43] but remains relatively unchanged irrespective of glycolaldehyde overlayer exposures $\leq$50 L_m. The water TPD spectra for the mixed glycolaldehyde:water ices are identical to those of the layers up to a composition of 20%. This behaviour would be expected if the cohesive energies of glycolaldehyde pure ices and between glycolaldehyde and water molecules are approximately the same. This assumption is supported by TPD (Figure 6) and RAIRS (Figure 7), which show similar spectra across all three ice configurations.

Our data show that the presence of COMs within water-rich interstellar ices at sufficient concentrations can potentially influence the desorption behaviour of the smaller and more volatile components of interstellar ices, since the desorption of these species is dictated by the water.[23] By inhibiting the crystallization of ASW, as observed for the acetic acid:water ices, and to a lesser extent for glycolaldehyde:water ices, volatiles will be retained within the ices to higher temperatures, and therefore remain within the ices for longer times. Similar effects have been observed for methanol containing water ices that retain OCS within the ice to higher temperatures.[50] As a consequence, these volatiles may undergo further surface processing and chemistry within the ices.

IV. ASTROPHYSICAL IMPLICATIONS AND CATEGORIZATION

Just as for smaller molecules commonly found in interstellar ices, understanding the basis of the trapping and desorption behaviour of COMs is important in developing more accurate astrophysical models.[5] In particular, laboratory studies of model interstellar ices allow a description of the desorption behaviour based on experimental observations. Given the large number of COMs that are considered to be important, it is useful to develop some general ideas that allow the classification of the desorption of more complex species. These generalisations describe thermal processes in the context of water-rich astrophysical ices. Actual astrophysical ices are multi-component in nature, however, our binary systems provide a useful guide to describe thermal processes of COMs in the presence of water ice. This water-dominated binary ice approach has been used previously by Collings *et al.*[23,28] to generalise the behaviour of a large range of smaller volatiles. The data we have recorded here, for three different isomers containing different functional groups, have allowed us to

develop classifications that can be applied to a range of C, H, and O containing COMs with different functional groups.

Of the three molecules investigated here, acetic acid has the strongest interactions with itself and with water, whilst methyl formate has the weakest interactions. Glycolaldehyde, on the other hand, is intermediate between the two. The origin of the observed desorption of these species from water ice can be assigned to the nature of the functional groups within the molecule, which dictate the sublimation temperature of the pure ices and govern the strength of the intermolecular interactions with water ice. For example, the carboxylic acid group in acetic acid facilitates hydrogen bonding with itself as well as with water, leading to a high desorption temperature for the pure ice[8] (greater than that of water) and to mainly co-desorption with water ice. This ability to hydrogen bond also allows the formation of a monolayer on the water ice surface, which is not observed for pure ices adsorbed on HOPG. In contrast, methyl formate contains an ester group which does not form strong intermolecular bonds, and hence the natural desorption temperature of the pure species is much lower compared to water and also when compared with acetic acid and glycolaldehyde. Methyl formate therefore mainly desorbs via a molecular volcano mechanism, with only a small amount of co-desorption being observed in water containing ice films. In addition, methyl formate can form weak interactions with water ice leading to an additional TPD peak due to the direct interaction of the C═O group with the water ice surface. Glycolaldehyde contains ketone and alcohol groups and can therefore bond to itself, as demonstrated by its ability to form dimers in the solid phase. However, the inter and intra-molecular interactions are weaker than those in acetic acid and hence its behaviour is intermediate between that of acetic acid and methyl formate. Glycolaldehyde primarily co-desorbs with water ice and also forms a monolayer on water, which is not observed for pure glycolaldehyde ice adsorbed on HOPG.

Based on the experimental observations described here, and those of other COMs recorded in our laboratory, we can use our data to classify the desorption of a molecule on the basis of its functional groups and therefore on its ability to directly interact with water ice. Collings *et al.* previously catalogued the desorption of a wide range of smaller molecules based on their behaviour when adsorbed on and in water ice.[23] The desorption of the molecules was divided into the following classifications: CO-like, water-like, or intermediate. For mixed ices, CO-like species show volcano and co-desorption features along with monolayer and multilayer desorption from the ice; water-like molecules show a single co-desorption peak coincident with water; intermediate species show the volcano and co-desorption peaks of trapped species, in addition to a minor desorption feature corresponding to the monolayer for molecules that are able to diffuse through ASW. These categorizations have subsequently allowed the modelling of a wide range of astrophysical environments.[28]

On the basis of the work described here, we have now extended these classifications to include C, H, and O containing COMs. Our new classifications are based on those derived previously,[23,28] but are extended to account for the stronger interactions of COMs with water due to the presence of functional groups that can bond directly to the water ice. Our classifications are as follows.

- **Complex intermediate species**: These include polar species which cannot form intermolecular hydrogen bonds, such as ketones, esters, ethers, aldehydes, and epoxides, and are predicted to show a lower desorption temperature for the pure species, when compared to water. These species exhibit mainly volcano desorption in the presence of water ice, with only small amounts of co-desorption. In many cases, these molecules also give rise to an additional desorption event due to their direct, but weak, interaction with water ice.
- **Complex water-like species**: Molecules which can form hydrogen bonds in the pure ice, such as carboxylic acids and alcohols, have desorption temperatures similar to (or higher than) that of water. The high natural desorption temperature limits the ability of the molecule to trap within water ice and hence mainly co-desorption is observed. For these species, thermally induced mixing of the molecule with water is also observed. These species may change the desorption profile and alter the crystallization of the water ice, depending on ice composition. For some molecules, a residue which remains on the surface after water desorption (as seen for acetic acid and glycine[48,49]) may also be observed, depending on ice composition.

Our complex intermediate classification extends that of Collings *et al.*,[23] by allowing for the additional desorption of a COM monolayer bonded to the water ice due to the direct interaction of the oxygen containing functional groups with the water. The complex water-like classification also extends the previous definition by taking into account the effect of the COM itself on water ice and the possibility of a residue remaining on the surface for species with higher desorption temperatures compared to water.

Table II shows the classifications of various COMs derived from our experimental results. These classifications were made on the basis of the desorption spectra of the $C_2O_2H_4$ isomers described here. We note that glycolaldehyde contains both aldehyde and hydroxyl functional groups, and forms intermolecular hydrogen bonds. Glycolaldehyde therefore behaves primarily as a complex-water-like species, although it does

TABLE II. Classifications of COMs on the basis of their desorption behaviour from water containing ices.

	Complex intermediate	Complex water-like
Experimental	Methyl formate Dimethyl ether Acetone	Acetic acid Ethanol Propan-2-ol Glycolaldehyde Methanol
Predictions	Methyl acetate Ethyl formate Ethylene oxide Propenal Propionaldehyde Acetaldehyde	Propan-1-ol Ethylene glycol Glycine Vinyl alcohol

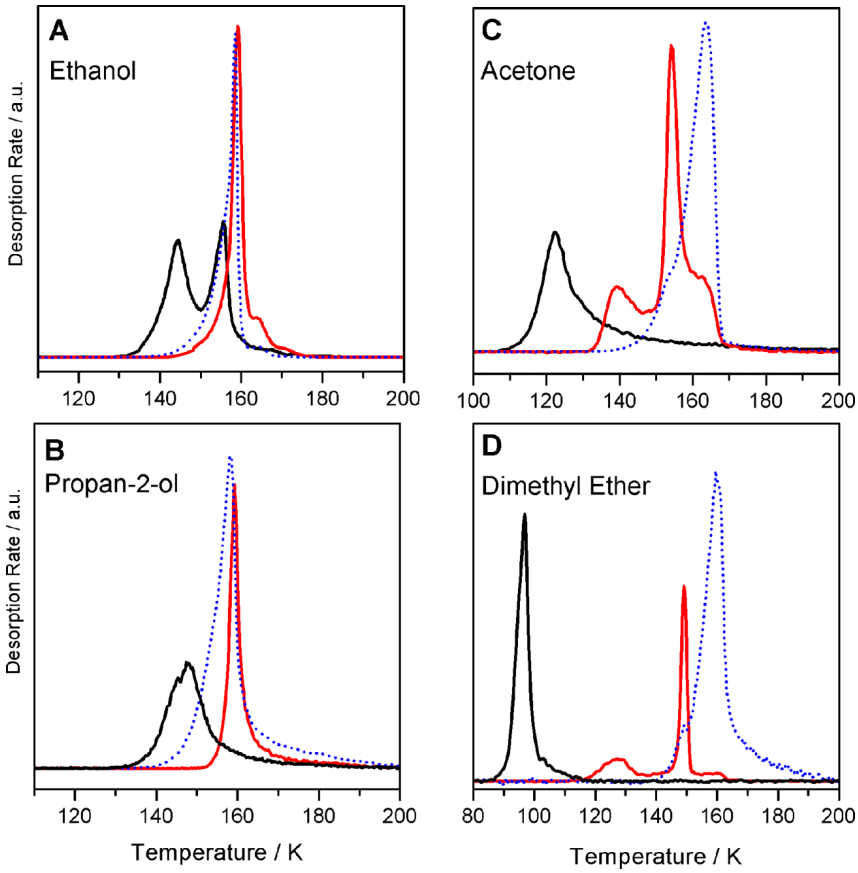

FIG. 9. TPD spectra for various COMs grown as co-deposited ice mixtures (red traces) adsorbed on HOPG at 23 K*. (a) Ethanol. (b) Propan-2-ol. (c) Acetone. (d) Dimethyl ether. In each case, the mixtures comprise of ~12%-15% of the COM, with respect to water. An equivalent exposure of a pure COM ice TPD (black trace) in addition to a scaled water TPD (dotted blue trace) are included in each panel for comparison. *Data in panel (a) were measured at 90 K.

show a minor volcano desorption component in mixed ices, as seen for complex intermediates.

To further test the validity of these classifications, we also recorded TPD spectra for the desorption of other C, H, and O containing COMs with 2 or more carbon atoms. Dimethyl ether, acetone, ethanol,[26] and propan-2-ol[54] were chosen because of their astrophysical relevance. In all cases, the desorption of these species was recorded both on and in water ice. Figure 9 shows representative TPD spectra for these molecules adsorbed in a co-deposited mixture with water ice. The concentration of the COMs is ~12%-15% with respect to water ice in all cases.

Figure 9 shows that both dimethyl ether and acetone (which would both be classified as complex intermediates on the basis of their functional groups) show exactly the expected behaviour, with the desorption from the mixtures being dominated by volcano desorption, as predicted. Furthermore, both species show an additional desorption event due to the direct interaction of the molecule with water ice. This is in agreement with the methyl formate TPD spectra reported here. In contrast, ethanol and propan-2-ol behave as expected for complex-water-like species. In both cases, desorption from the mixtures is clearly dominated by complete co-desorption with water. Table II also includes methanol. Despite this only containing a single carbon atom, it has been included based on its importance in astrochemistry and ubiquity across astrophysical environments. Methanol was previously categorized as water-like by Collings *et al.*,[23] however, based on our previous results[44,50] its classification is extended to complex water-like. This takes into account the observation that methanol directly affects the crystallisation of water.

Table II also contains predictions for additional COMs, which are classified based on their structure and functional groups. Again, the COMs were chosen based on their astrophysical importance either observationally and/or as precursors in chemical networks leading to the formation of more complex pre-biotic species, see, for example, Refs. 1 and 5. Due to the presence of hydroxyl groups, propan-1-ol, ethylene glycol, glycine, and vinyl alcohol are predicted to behave as complex water-like species. TPD data recorded for glycine adsorbed on ASW support this prediction.[48,49] Preliminary data recorded in our laboratory for pure ethylene glycol adsorbed on HOPG show that it desorbs ~30 K higher than water ice, again supporting this classification.

Methyl acetate, ethyl formate, ethylene oxide, propenal, propanal, and acetaldehyde are all predicted to behave as complex intermediate species. This is based on the presence of ester, aldehyde, and epoxide functional groups. Methyl acetate and ethyl formate have been shown to exhibit similar desorption behaviour to that of methyl formate when adsorbed on metal surfaces,[33] supporting these predictions, whilst ethylene oxide has previously been classified as an intermediate species by Occhiogrosso *et al.*[55] Since ethylene oxide contains an epoxide functional group, it is probable that this molecule will show an additional desorption feature due to the interaction with water ice and hence we extend the classification of ethylene oxide to a complex intermediate species.

V. CONCLUSIONS

TPD and RAIRS have been used to probe the interactions of the three isomers of $C_2O_2H_4$ with various water ice configurations at astrophysically relevant temperatures (20 K). A range of ice compositions and configurations that includes water-rich ASW, CI, and co-deposited mixtures has allowed a detailed comparative study to be undertaken. The desorption behaviour of glycolaldehyde, methyl formate, and acetic acid has been categorized based on the work of Collings *et al.* who studied the sublimation trends of a wide range of small molecules from water ices. These original classifications have been extended to accommodate the more complex interactions of COMs with the water ice based on their functional groups, sublimation temperatures, and effects on water crystallization and desorption processes.

Methyl formate has been classified as a complex intermediate. The desorption behaviour in the presence of water is similar to smaller volatile species, e.g., CO_2, and is dominated by desorption at the ASW to CI phase transition with a limited co-desorption component. The oxygen containing functional group gives rise to an additional interaction with water, thus differentiating it from the original intermediate class defined by Collings *et al.* Similar behaviour is also observed for the simplest ketone (acetone) and ether (dimethyl ether). Hence, it is predicted that other simple esters, ketones, and ethers exhibit the same desorption behaviour.

Acetic acid and glycolaldehyde have been classified as complex water-like species. The desorption behaviour of these molecules in the presence of water is dominated by co-desorption. Furthermore, these molecules directly affect the crystallization of water and therefore may change the overall desorption behaviour of multi-component ices.[50] In this case, the carboxylic acid and alcohol functional groups facilitate hydrogen bonding to the water ice. The ability of these species to directly hydrogen bond to water alters the desorption kinetics of surface bound species with monolayers forming on water ice surfaces for both acetic acid and glycolaldehyde. This is not seen for the pure ices adsorbed on HOPG.[8] Similar desorption behaviour is observed for simple alcohols, including ethanol and propan-2-ol, with other alcohols predicted to follow the same trends.

ACKNOWLEDGMENTS

The Leverhulme Trust is thanked for funding D.J.B. and P.M.W. to undertake this research at UCL and the University of Sussex is thanked for further funding for D.J.B. at Sussex. F.P. acknowledges support from the European Community's Seventh Framework Programme No. FP7/2007-2013 under Grant Agreement No. 238258. Sean Ayling, James Martin, and Charlie Barty-King are thanked for recording the TPD spectra for propan-2-ol, acetone, and dimethyl ether in Figure 9.

[1]E. Herbst and E. F. van Dishoeck, Annu. Rev. Astron. Astrophys. **47**, 427 (2009).
[2]A. Coutens, M. V. Persson, J. K. Jorgensen, S. F. Wampfler, and J. M. Lykke, Astron. Astrophys. **576**, A5 (2015).
[3]H. Calcutt, S. Viti, C. Codella, M. T. Beltran, F. Fontani, and P. M. Woods, Mon. Not. R. Astron. Soc. **443**, 3157 (2014).
[4]N. Biver, D. Bockelée-Morvan, V. Debout, J. Crovisier, J. Boissier, D. C. Lis, N. Dell Russo, R. Moreno, P. Colom, G. Paubert, R. Vervack, and H. A. Weaver, Astron. Astrophys. **566**, 4 (2014).
[5]R. T. Garrod and S. L. Widicus, Weaver, Chem. Rev. **113**, 8939 (2013).
[6]M. Bertin, C. Romanzin, X. Michaut, P. Jeseck, and J.-H. Fillion, J. Phys. Chem. C **115**, 12920 (2011).
[7]D. J. Burke, F. Puletti, W. A. Brown, P. M. Woods, S. Viti, and B. Slater, Mon. Not. R. Astron. Soc. **447**, 1444 (2015).
[8]D. J. Burke, F. Puletti, P. M. Woods, S. Viti, B. Slater, and W. A. Brown, J. Phys. Chem. A **119**, 6837 (2015).
[9]S. Maity, R. I. Kaiser, and B. M. Jones, Faraday Discuss. **168**, 485 (2014).
[10]C. J. Bennett, S. H. Chen, B. Sun, A. H. H. Chang, and R. I. Kaiser, Astrophys. J. **660**, 1588 (2007).
[11]G. Fedoseev, H. M. Cuppen, S. Ioppolo, T. Lamberts, and H. Linnartz, Mon. Not. R. Astron. Soc. **448**, 1288 (2015).
[12]P. Modica, M. E. Palumbo, and G. Strazzulla, Planet. Space Sci. **73**, 425 (2012).
[13]P. Modica and M. E. Palumbo, Astron. Astrophys. **519**, A22 (2010).
[14]K. I. Öberg, R. T. Garrod, E. F. van Dishoeck, and H. Linnartz, Astron. Astrophys. **504**, 891 (2009).
[15]H. J. Cleaves II, in *Encyclopedia of Astrobiology*, 1st ed., edited by M. Gargaud, R. Amils, J. Cernicharo Quintanilla, H. J. Cleaves, W. M. Irvine, D. Pinti, and M. Viso (Springer-Verlag, Berlin, 2011), p. 600.
[16]Z. Peeters, S. D. Rodgers, S. B. Charnley, L. Schriver-Mazzuoli, A. Schriver, J. V. Keane, and P. Ehrenfreund, Astron. Astrophys. **445**, 197 (2006).
[17]P. M. Woods, B. Slater, Z. Raza, S. Viti, W. A. Brown, and D. J. Burke, Astrophys. J. **777**, 90 (2013).
[18]P. M. Woods, G. Kelly, S. Viti, B. Slater, W. A. Brown, F. Puletti, D. J. Burke, and Z. Raza, Astrophys. J. **750**, 19 (2012).
[19]A. Occhiogrosso, S. Viti, P. Modica, and M. E. Palumbo, Mon. Not. R. Astron. Soc. **418**, 1923 (2011).
[20]R. T. Garrod, Astrophys. J. **765**, 60 (2013).
[21]E. L. Gibb, D. C. B. Whittet, A. C. A. Boogert, and A. G. G. M. Tielens, Astrophys. J., Suppl. Ser. **155**, 35 (2004).
[22]P. Ayotte, R. S. Smith, K. P. Stevenson, Z. Dohnálek, G. A. Kimmel, and B. D. Kay, J. Geophys. Res. **106**, 387, doi:10.1029/2000je001362 (2001).
[23]M. P. Collings, M. A. Anderson, R. Chen, J. W. Dever, S. Viti, D. A. Williams, and M. R. S. McCoustra, Mon. Not. R. Astron. Soc. **354**, 1133 (2004).
[24]A. Bar-Nun, I. Kleinfeld, and E. Kochavi, Phys. Rev. B **38**, 7749 (1988).
[25]A. J. Wolff, C. Carlstedt, and W. A. Brown, J. Phys. Chem. C **111**, 5990 (2007).
[26]D. J. Burke, A. J. Wolff, J. L. Edridge, and W. A. Brown, Phys. Chem. Chem. Phys. **10**, 4956 (2008).
[27]R. Souda, Phys. Rev. B **75**, 184116 (2007).
[28]S. Viti, M. P. Collings, J. W. Dever, M. R. S. McCoustra, and D. A. Williams, Mon. Not. R. Astron. Soc. **354**, 1141 (2004).
[29]P. M. Woods, A. Occhiogrosso, S. Viti, Z. Kanuchova, M. E. Palumbo, and S. D. Price, Mon. Not. R. Astron. Soc. **450**, 1256 (2015).
[30]R. S. Smith, J. Matthiesen, and B. D. Kay, J. Phys. Chem. A **118**, 8242 (2014).
[31]R. L. Hudson, M. H. Moore, and A. M. Cook, Adv. Space Res. **36**, 184 (2005).
[32]A. L. Schwaner, J. E. Fieberg, and J. M. White, J. Phys. Chem. B **101**, 11112 (1997).
[33]E. Zahidi, M. Castonguay, and P. McBreen, J. Am. Chem. Soc. **116**, 5847 (1994).
[34]B. A. Sexton, A. E. Hughes, and N. R. Avery, Surf. Sci. **155**, 366 (1985).
[35]M. Lattelais, M. Bertin, H. Mokrane, C. Romanzin, X. Michaut, P. Jeseck, J.-H. Fillion, H. Chaabouni, E. Congiu, F. Dulieu, S. Baouche, J.-L. Lemaire, F. Pauzat, J. Pilmé, C. Minot, and Y. Ellinger, Astron. Astrophys. **532**, A12 (2011).
[36]Q. Gao and K. T. Leung, J. Phys. Chem. B **109**, 13263 (2005).
[37]S. Bahr, A. Borodin, O. Höfft, V. Kempter, A. Allouche, F. Borget, and T. Chiavassa, J. Phys. Chem. B **110**, 8649 (2006).
[38]A. Allouche and S. Bahr, J. Phys. Chem. B **110**, 8640 (2006).
[39]S. Hellebust, B. O'Riordan, and J. Sodeau, J. Chem. Phys. **126**, 084702 (2007).
[40]R. Souda, Chem. Phys. Lett. **413**, 171 (2005).
[41]P. Jenniskens and D. F. Blake, Science **265**, 753 (1994).
[42]R. Wiesendanger, L. Eng, H. R. Hidber, P. Oelhafen, L. Rosenthaler, U. Staufer, and H.-J. Guntherodt, Surf. Sci. **189/190**, 24 (1987).
[43]R. S. Smith, C. Huang, E. K. L. Wong, and B. D. Kay, Phys. Rev. Lett. **79**, 909 (1997).

[44]D. J. Burke and W. A. Brown, Phys. Chem. Chem. Phys. **12**, 5947 (2010).
[45]A. S. Bolina, A. J. Wolff, and W. A. Brown, J. Phys. Chem. B **109**, 16836 (2005).
[46]D. Chakarov, L. Österlund, and B. Kasemo, Vacuum **46**, 1109 (1995).
[47]J. L. Edridge, K. Freimann, D. J. Burke, and W. A. Brown, Philos. Trans. R. Soc., A **371**, 20110578 (2013).
[48]G. Tzvetkov and F. P. Netzer, Chem. Phys. Lett. **588**, 109 (2013).
[49]G. Tzvetkov, G. Koller, and F. P. Netzer, Surf. Sci. **606**, 1879 (2012).
[50]D. J. Burke and W. A. Brown, Mon. Not. R. Astron. Soc. **448**, 1807 (2015).
[51]E. Backus, M. Grecea, A. Kleyn, and M. Bonn, Phys. Rev. Lett. **92**, 236101 (2004).
[52]W. Hagen, A. G. G. M. Tielens, and J. M. Greenberg, Chem. Phys. **56**, 367 (1981).
[53]G. Notesco and A. Bar-Nun, Icarus **126**, 336 (1997).
[54]S. A. Ayling, D. J. Burke, and W. A. Brown, "The surface chemistry of propan-2-ol and water on graphite at 20 K" (unpublished).
[55]A. Occhiogrosso, A. Vasyunin, E. Herbst, S. Viti, M. D. Ward, S. D. Price, and W. A. Brown, Astron. Astrophys. **564**, A123 (2014).